Optimization of DPF Structures with a 3D-Unit Cell Model

Wieland Beckert, Marcel Dannowski, Lisabeth Wagner, Jörg Adler, Lars Mammitzsch
Fraunhofer IKTS, Dresden, Germany
*Corresponding author: FhG IKTS, 01277 Dresden, Winterbergstrasse 28, wieland.beckert@ikts.fraunhofer.de

Abstract: The performance of Diesel Particulate Filters is evaluated by pressure drop and soot charge capacity during operation and is controlled by the properties of the porous wall material (permeability, pore distribution, max. soot charge) and the geometry (channel-shape,-length, wall thickness) of the filter structure [1]. The manufacturing of ceramic filter segments proceeds over an extrusion process and requires expensive design specific tools. An empirical optimization with trial and error cycles in the hardware is extremely costly: a "virtual" optimization process via simulation is more promising [2]. Aim of the presented model is to analyze the influence of filter structure and material parameters on flow and soot deposition. The model geometry consists of a 3D unit cell of a typical ceramic particulate filter. Physical mechanisms included are free (channels) and porous (wall) gas flow, convective mass flow (gas soot concentration) and mass deposition (soot concentration in porous wall, soot cake formation) of soot. A comparison of model predictions with experimental results proved the validity and the applicability of the model for virtual design purposes.

Keywords: diesel particulate filter, ceramics, fluid flow analysis, design optimization

1. Introduction

A typical ceramic particulate filter, as used for soot particle reduction in exhaust gases, consists of a monolithic porous ceramic body with a uniformly distributed structure of neighbored inlet and outlet channels. The soot-laden exhaust gas enters the filter at the end blocked inlet channels, so that the flow is forced through their porous side walls towards the outlet channels, lying in parallel (having a blocked inlet), and leaves them purged on the opposing open ends (figure 1). The soot particles are adsorbed at the pore walls, thereby gradually reducing the permeability of the porous structure with time. After reaching a saturation maximum load value near to the walls inlet surface the filtering mode is changing and a soot cake starts to grow on the porous wall, contributing to the perpendicular flow resistance of the walls and gradually reducing the free flow section of the inlet walls.

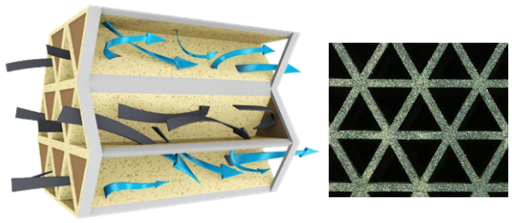

Figure 1. Ceramic particle filter concept (left, from www.huss-group.com) and structure (right, IKTS)

Manufacturers have the choice between various geometrical design variants, differing by shape and arrangement of the filter channels (figure 2).

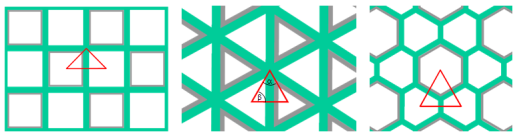

Figure 2. Ceramic particle filter design concepts (cell arrangement with unit cell)

Both general design type (rectangular, triangular, hexagonal,...) and the specific geometrical parameters (channel diameter, length, wall thickness, ...) have an effect of filter back-pressure and particle loading capacity, together with the porous material specifications (pore distribution, permeability...). Due to the regular arrangement of filter channels it is possible to restrict the model analysis to a repeating unit cell geometry by applying symmetry relations [2]. This corresponds to an idealized approach of an infinite extended filter under uniform flow and ignores effect of exhaust gas distribution and filter housing but it is adequate for an evaluation of the cell structure.

2. Numerical Model

Comsol 3.5a was applied as computational platform for the model. Three different geometrical design variants have been investigated: the

rectangular, the triangular and the hexagonal cell design type. While for the rectangular and the hexagonal type the model was restricted to the analysis of an empty filter without soot load, for the triangular design the model was further extended to a full analysis with soot load in a following step. For the empty filters the cell geometry was complemented by an gas collector domain in front and a gas expansion zone behind the filter, considering the pressure contributions from the dynamic, inertia flow effects (figure 3).

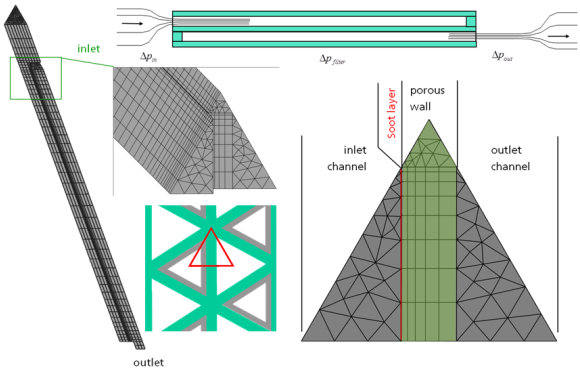

Figure 3. Geometry and mesh for analysed DPF unit cell variant with triangular channels (b_{cell}=1.63 mm; l_{cell}= 150-260 mm)

In the full model, involving soot transport effects, these domains were switched inactive, to reduce computational efforts and corresponding corrections of the inlet and outlet pressure level (derived from the empty filter analyses) were externally added to the results. The full model contains an additional domain between inlet channel and porous wall domain, representing the growing soot cake, which thickness was changed during transient model analysis by an moving mesh approach, controlled by the local evolution of soot cake thickness h_{soot}. (figure 4). The model applied free surface meshes of the channel sections which were swept along the channel length direction.

The model distinguishes between an inlet channel domain $^{(in)}$, an outlet channel domain $^{(out)}$, a porous wall domain $^{(wall)}$ and the soot cake domain $^{(cake)}$. In the inlet and the outlet channel domain Navier-Stokes-Flow is the only relevant physical mode; soot gas concentration is considered constant and a particular DOF is therefore not necessary. The porous wall domain contains a Darcy mode for gas flow and two reduced convection-diffusion mass transport modes accounting for soot mass concentration in the gas , $\rho_{soot}^{(gas)}$, and in the wall, $\rho_{soot}^{(wall)}$. The soot charging state of the porous structure is described by the ratio $\xi_{soot}^{(wall)} = \rho_{soot}^{(wall)} / \rho_{soot,\max}^{(wall)}$ $(0 \le \xi_{soot}^{(wall)} \le 1)$. The flow permeability of the porous wall is a function of the initial permeability, $\kappa_0^{(wall)}$ of the empty ceramic material, and the soot saturation ratio: $\kappa^{(wall)} = \kappa_0^{(wall)} \cdot f\left(\xi_{soot}^{(wall)}\right)$. The inlet boundary condition (homogeneous initial soot load, $\rho_{soot,0}^{(gas)}$) of the exhaust gas soot concentration is applied as a boundary condition directly to the inlet side surface of the porous wall; the outlet side corresponds to purely convective flux.

The soot cake domain takes part in the continuous gas flow (Darcy mode) through the whole model and is described by a thickness, h_{soot}, a constant, bulk soot mass density value $\rho_{soot}^{(cake)}$ and flow permeability $\kappa_{soot}^{(cake)}$. Initially, it has a very small thickness and a high initial permeability value with a neglecting influence on gas flow. After the soot charging state reaches a saturation value $\xi_{soot}^{(wall,surf)} \to 1$ at the neighbored surface of the porous wall, a smoothed triggering function $\Phi\left(\xi_{soot}^{(wall)}\right): 0 \overset{\xi_{soot}^{(wall,surf)} \to 1}{\to} 1$ switches soot deposition from wall deposition to soot cake deposition. The soot concentration at the porous wall inlet is switched to zero and the incoming soot mass rate at the soot cake is completely deposited there. This is accounted for by an separate DOF and an accumulation balance for h_{soot} in the soot cake domain. This variable controls a moving mesh mode, extending the local perpendicular dimension of the soot cake layer and reducing the free flow area of the inlet channel.

While for the empty filter cases stationary analyses were sufficient, for the soot loading models transient analyses were employed. To reproduce the operation mode of the experimental investigations with a constant exhaust gas flow rate over time, a kind of integrating (I)-controller implementation was applied for the inlet pressure by help of a corresponding global equation $p_{in} = K \cdot \left(\dot{V}_{in}^{(act)} - \dot{V}_{in}^{(set)}\right)$.

For all analyzed cases laminar flow conditions were satisfied.

3. Governing Equations

Gas-Flow:

continuity equation:

$$\nabla \cdot (\rho \cdot \mathbf{v}) = 0 \qquad (1)$$

compressible Navier-Stokes: (inlet/ outlet domains)

$$\rho \cdot (\mathbf{v} \cdot \nabla)\mathbf{v} + \nabla p - \mu \cdot (\Delta \mathbf{v} + \nabla(\nabla \cdot \mathbf{v})) = 0 \qquad (2)$$

Darcy: (porous wall, soot cake)

$$\nabla p = -\frac{\mu}{\kappa^{(wall)}} \cdot \mathbf{v} \qquad (3)$$

soot mass concentration gas (porous wall):

$$\mathbf{v}_{gas} \cdot \left(\nabla \cdot \rho_{soot}^{(gas)}\right) = -\dot{S}_{soot} \qquad (4)$$

soot mass concentration wall (porous wall)

$$\dot{\rho}_{soot}^{(wall)} = +\dot{S}_{soot} \qquad (5)$$

soot deposition rate (porous wall)

$$\dot{S}_{soot} = R_{soot,0}^{(wall)} \cdot \rho_{soot}^{(gas)} \cdot |\mathbf{v}| \qquad (6)$$

rate equation for soot cake thickness (soot cake)

$$\dot{h}_{soot} = \Phi \cdot |\mathbf{v}_n| \cdot \rho_{soot}^{(gas)} / \rho_{soot}^{(cake)} \qquad (7)$$

The balances (4), (5), (7) were implemented by convection/diffusion modes and had to become numerically stabilized by virtual diffusion terms. The various model parameters describing soot and ceramic behavior were obtained from an experimental characterization campaign with specially made, soot charged disc samples from the porous filter material.

4. Model results

4.1 Empty filter analysis

A typical result for the pressure and velocity variations along the inlet and the outlet channel of an (empty) filter cell is depicted in figure 4 where the results from the 3D model are compared with that from a simpler 1D-model based on a pure viscous pipe flow approach. The large differences are due to the dynamic pressure effects from the consideration of the gas inertia terms of the Navier-Stokes approach especially present in the inlet channel. The 3D analysis proved that the existing simple 1D-model was inadequate for higher flow rates.

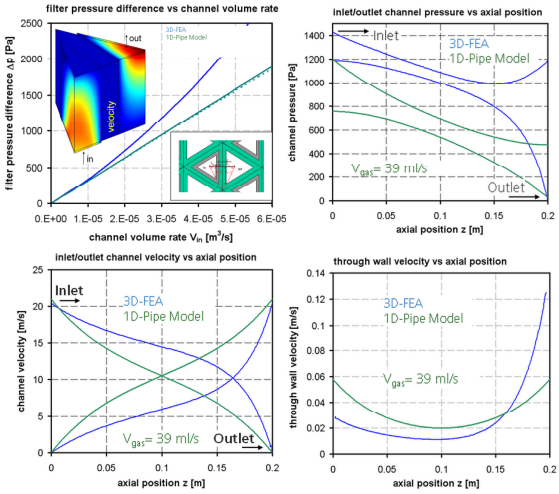

Figure 4. Results from the 3D-FE model (blue) compared with that of an older, simpler 1D-viscous-pipe flow model (green) of an empty filter for (top left) total pressure vs. flow rate, (top right) in/out-channel pressure, (bottom left) in-out-channel velocity vs. axial position, (bottom right) through wall velocity vs. axial position

Since the transverse flow through the filter walls is driven by the local pressure difference between inlet and outlet channel, the wall flow distribution (and therefore, later, the soot deposition) is distinctly inhomogeneous along the filter length.

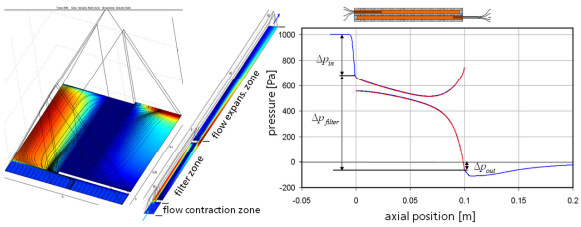

Figure 5. Dynamic pressure contribution from flow contraction (inflow zone) and flow expansion (outflow zone) as obtained for an example load case from the model (left: 3D plot from the model for velocity results in truely and anisotropically scaled presentation)

Figure 5 shows the additional contributions of contraction flow (inflow zone) and expansion (outflow zone) to total filter back pressure, which is from the same order of magnitude as that for the filter structure itself and has to be considered in the analyses. The values may be extracted from the empty filter models for a given geometry and flow rate and externally applied

to the results of the soot loading analyses which were carried out at the detached cell geometries.

The model was used to analyze the influence of ceramic material (wall permeability) and geometric parameters (e.g. filter channel length) on the filter behavior. One example for corresponding results can be found in figure 6, where the internal distribution of gas pressure in the cell channels is depicted for two different material variants (A and B) and two filter length (6 inch and 8 inch).

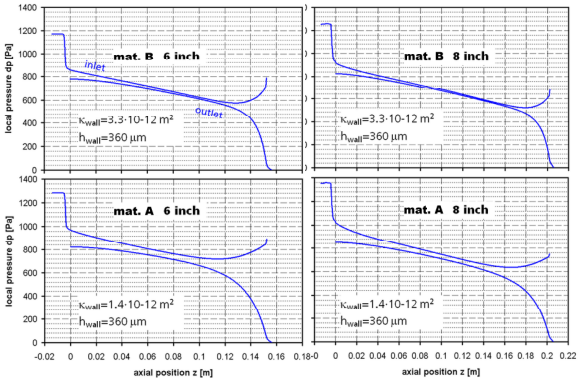

Figure 6. Model and experimental results for filter pressure characteristics for filter with varying length (filter segment exhaust gas flow rate 200 l/min).

Figure 7 compares model predictions with experimental results obtained from actual filter segments (triangular cell type) and varying filter lengths. The evaluation proved a good validity of the model. The deviations can be contributed to the tolerances of the filter channel geometry (channel width, wall thickness) compared to the manufacturers specifications.

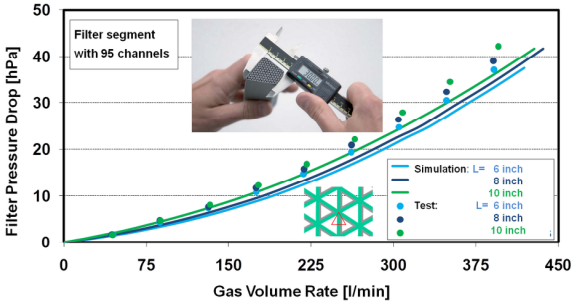

Figure 7. Model and experimental results for filter pressure characteristics from filters with varying length.

4.2 Soot loading analyses

In the following the analysis was extended from the empty filter case to the consideration of the soot loading process. The filter cell was loaded by a constant exhaust gas flow rate with a given soot concentration and the changes of the quantities ($\rho_{soot}^{(gas)}, \rho_{soot}^{(wall)}$, h_{soot} $p^{(in/out)}$, $\kappa^{(wall)}$...) by soot deposition in the porous wall, and after saturation, in a soot cake growing at the inlet wall were analyzed on the local scale over time in a transient study.

In a first approach the geometrical effect of soot cake formation on the free section of the inlet flow channel had been ignored. The soot cake layer thickness was kept constant (without moving mesh) and only the increase in pressure drop from transverse flow through the soot cake was considered by scaling of the soot cake permeability.

Figure 8 illustrates the soot loading process: soot deposition rates are directly proportional to wall flow speed and therefore highest at the end of the inlet channel. With increasing depth from the wall surface, soot concentration in the gas flow is reduced and deposition rate decreases. Soot charge saturation therefore begins from the inlet surface near the end of the inlet channel and a soot cake starts to grow there. With increasing time, soot saturation moves continuously forwards in the direction of the entry of the inlet channel. After some time the whole inlet surface of the porous wall is covered by a continuous soot cake with a thickness distribution slowly smoothing out.

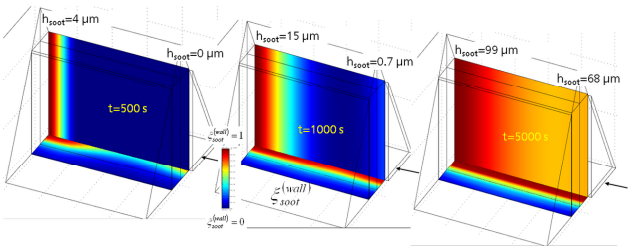

Figure 8. Evolution of wall soot saturation ratio and soot cake layer thickness with time for a filter with length 0.2m .

Figure 9 shows the change in global pressure characteristics, if the additional effect from the reduction of the inlet section is considered in the analysis by applying a moving mesh approach to

the soot cake layer domain. The soot cake has a distinct effect on the flow and the pressure loss in the inlet channel. The correspondence to experimental data is better and can be further improved by a correction of the assumption for the soot cake permeability from $\kappa_{soot}^{(cake)} = 0.13\ \mu m^2$ to $\kappa_{soot}^{(cake)} = 0.06\ \mu m^2$.

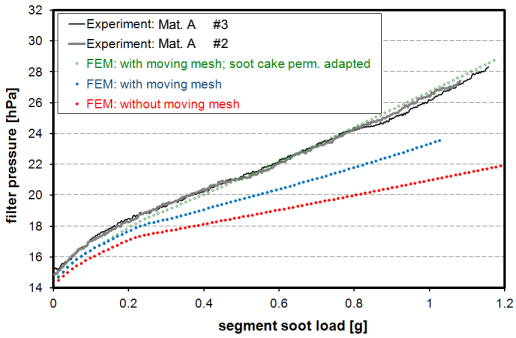

Figure 9. Model and experimental results for the evolution of filter pressure with filter segment soot load (Length 6 inch). Considering the inlet channel variation from soot cake growth (blue, green) increases the pressure compared with ignoring its influence (red). Adapting assumption for soot cake permeability from 0.13 to 0.08 μm^2 further improves model validity.

The model also easily provides a partition of the total soot charge of the filter to the different deposition modes as is illustrated in figure 11.

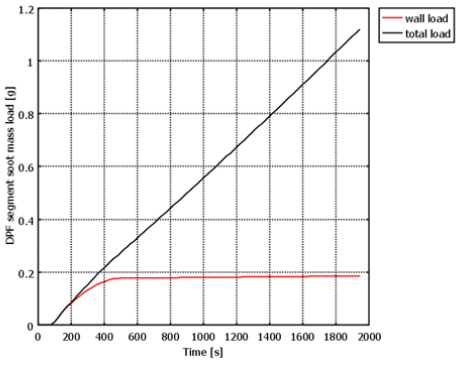

Figure 10. Evolution of wall (red) and total (black) soot mass deposition with time for a DPF segment.

Finally the results of an experimental characterization campaign from real filter segments with a triangular cell design was compared with the model predictions for the soot charging behavior in figure 11. The available data set contains measurements for 2 different material types (A and B) and 2 different filter segment lengths (6 inch and 8 inch). The corresponding model results agree quite well with the experimental data, correctly reproducing the trends of the influence of the different design parameters (material: permeability, geometry: filter length). The coincidence could be probably further improved, especially by a more elaborate characterization of the set of soot related parameters.

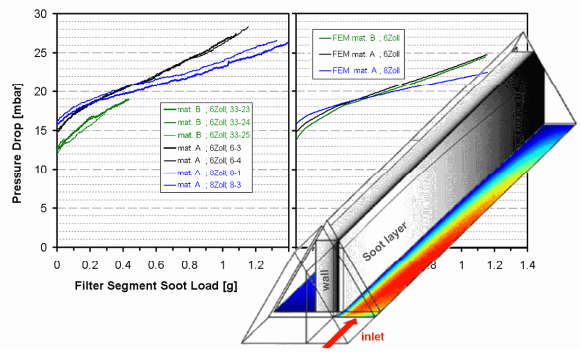

Figure 11. Comparison of model predictions (right) and experimental results for the evolution of filter pressure with soot load for filter segments from different materials and length (6 inch, 8 inch). The overlaid sketch combines model results for channel gas velocity (color level), wall soot saturation ratio (gray level wall) and soot cake layer thickness (gray level + mesh displacement). Parameter set from disc samples used.

In the present study their values were obtained from soot charging measurements with macroscopic ceramic disc samples. Since manufacturing is different and the geometric dimensions are fare away from the conditions in the mesoscopic small filter channels the obtained parameters may be not fully comparable. An alternative way could be an estimation from microstructural computational modeling methods based on a synthetic representation of the materials microstructure and a detailed description of the physical mechanisms of soot deposition. Corresponding possibilities are offered for instance from the GeoDict/ FilterDict software of Fraunhofer ITWM [3]. The results of a corresponding cooperation between IKTS and ITWM, (FeiFilTools [3]), analyzing the soot particle deposition process in a porous ceramic with advanced microstructural models together with elaborate experimental characterization techniques has been already accomplished for the materials investigated in this study. It provides a data basis

for future work to obtain better estimates for the parameters of the soot deposition process needed in the presented model.

5. Conclusions

The model approach offers an efficient tool to analyze the influences of geometrical design (channel shape and arrangement, filter length, wall thickness) and filter material properties (permeability, soot loading characteristics) on the performance of ceramic particle filter structure in the soot loading process, assessed by pressure loss and soot loading capacity. It does correctly predict the corresponding relations and trends as could be proved from an experimental evaluation. An application of the model as a virtual tool for efficient optimization of a filter structure towards user target values for an specific application could help to avoid expensive practical trial and error loops with costly adaptions of real tools.

Chances to improve the model are seen in more realistic evaluations of the parameters and relations related to soot deposition. In this regard the current model relies on very simple empirical assumptions and on parameters obtained from macroscopic disc samples, which may be not fully comparable to the specific conditions on the channel scale. A promising alternative is seen in a hierarchical multiscale modeling approach, where the soot deposition characteristics are obtained from an advanced microscale model analysis with specific simulation tools. A corresponding cooperation with the Fraunhofer ITWM, utilizing their GeoDict and FilterDict software, is under way and provided interesting results.

6. References

1. J. Adler, Ceramic diesel particulate filters, *International Journal of Applied Ceramic Technology*, **2**, pp. 429–439 (2005)
2. A.G. Konstandopoulos et al, Advances in the science and technology of Diesel particulate filter simulation, *Adv.Chem. Eng.*, **33**, 284–294 (2007)
3. S. Rief et al. Virtual Diesel Particulate Filters: Simulation of the Structure, Exhaust Gas Flow and Particle Deposition, *Filtration*, **9**, 315-320 (2009)

7. Acknowledgements

We thank the Fraunhofer Society for funding this work in the FeiFilTools MEF project.